10752 *Biochemistry* **2009,** *48,* 10752–10764
DOI: 10.1021/bi901400p

BIOCHEMISTRY
including biophysical chemistry & molecular biology
Article

Directed "*in Situ*" Inhibitor Elongation as a Strategy To Structurally Characterize the Covalent Glycosyl-Enzyme Intermediate of Human Pancreatic α-Amylase[†,‡]

Ran Zhang,[§,⊥] Chunmin Li,[§,∥] Leslie K. Williams,[∥] Brian P. Rempel,[⊥] Gary D. Brayer,[∥] and Stephen G. Withers*[,⊥,∥]

[∥] *Department of Biochemistry and Molecular Biology, University of British Columbia, Vancouver, British Columbia V6T 1Z3, Canada, and* [⊥] *Department of Chemistry, University of British Columbia, Vancouver, British Columbia V6T 1Z1, Canada.* [§] *These authors contributed equally to this work.*

Received August 12, 2009; Revised Manuscript Received October 4, 2009

ABSTRACT: While covalent catalytic intermediates of retaining α-transglycosylases have been structurally characterized previously, no such information for a hydrolytic α-amylase has been obtained. This study presents a new "*in situ*" enzymatic elongation methodology that, for the first time, has allowed the isolation and structural characterization of a catalytically competent covalent glycosyl-enzyme intermediate with human pancreatic α-amylase. This has been achieved by the use of a 5-fluoro-β-L-idosyl fluoride "warhead" in conjunction with either α-maltotriosyl fluoride or 4′-*O*-methyl-α-maltosyl fluoride as elongation agents. This generates an oligosaccharyl-5-fluoroglycosyl fluoride that then reacts with the free enzyme. The resultant covalent intermediates are extremely stable, with hydrolytic half-lives on the order of 240 h for the trisaccharide complex. In the presence of maltose, however, they undergo turnover via transglycosylation according to a half-life of less than 1 h. Structural studies of intermediate complexes unambiguously show the covalent attachment of a 5-fluoro-α-L-idosyl moiety in the chair conformation to the side chain of the catalytic nucleophile D197. The elongated portions of the intermediate complexes are found to bind in the high-affinity −2 and −3 binding subsites, forming extensive hydrogen-bonding interactions. Comparative structural analyses with the related noncovalent complex formed by acarbose highlight the structural rigidity of the enzyme surface during catalysis and the key role that substrate conformational flexibility must play in this process. Taken together, the structural data provide atomic details of several key catalytic steps. The scope of this elongation approach to probe the active sites and catalytic mechanisms of α-amylases is further demonstrated through preliminary experiments with porcine pancreatic α-amylase.

Human pancreatic α-amylase (HPA)[1] is a key endoglycosidase involved in the digestion of dietary starch in the gut, generating a mixture of oligosaccharides, including maltose and a variety of α-(1−4)- and α-(1−6)-branched oligoglucans that are then further hydrolyzed to glucose by other glucosidases. Consequently, the activity of HPA in the small intestine has been shown to directly correlate with postprandial sugar levels in the bloodstream (*2*−*5*). Control of the activity of HPA thus provides a valuable therapeutic approach for diseases such as diabetes and obesity. Indeed, several α-glucosidase inhibitors (acarbose, miglitol, and voglibose) have been used clinically for the treatment of type II diabetes. However, their nonspecific binding to a wide range of glucosidases leads to undesirable side effects, limiting their effectiveness. A better understanding of the structure and mechanism of action of HPA would therefore help in the design of more specific inhibitors for therapeutic use.

HPA is a member of glycoside hydrolase family GH13 in the CAZy classification system (*6*, *7*). This family primarily contains enzymes acting on α-glycosidic linkages such as α-amylases, pullulanases, cyclodextrin glucanotransferases, amylosucrases, and α-glucosidases. Although overall sequence homology is relatively low between members of this family, their three-dimensional structures are fairly well conserved. HPA typifies such structures with its three domains (*8*). Domain A has an $(\alpha/\beta)_8$ barrel structure and contains the active site, along with an essential chloride ion binding site, which is thought to modulate the electrostatic environment of the active site (*9*−*11*). Domain B protrudes from the side wall of domain A and forms a calcium binding site. Domain C has an antiparallel β-barrel-type structure of unknown function, though a role in starch binding seems possible. Substrate mapping studies reveal at least five high-affinity glucose binding subsites within the active site, with three on the nonreducing side of the scissile bond and two sites on the reducing end side (*12*). This has been supported by several three-dimensional structures of this enzyme in complex with a range of substrates and inhibitors (*13*).

Three essential carboxylic acid residues are conserved in HPA and throughout the family GH13 enzymes (*14*). Structural

[†] This work was supported by an operating grant from the Canadian Institutes for Health Research (CIHR). R.Z. is the recipient of the British Columbia Innovation Council (BCIC) Innovation Scholarship. L.K.W. is supported by a Natural Sciences and Engineering Research Council of Canada Scholarship (NSERC).

[‡] Coordinates for the three structures described in this work have been deposited in the Protein Data Bank (*1*): MeG2F/5FIdoF/HPA (condition 1), PDB code 3IJ8; G3F/5FIdoF/HPA (condition 2), PDB code 3IJ9; MeG2F/5FIdoF/HPA (condition 3), PDB code 3IJ7.

*To whom correspondence should be addressed. Tel: 604-822-3402. Fax: 604-822-8869. E-mail: withers@chem.ubc.ca.

[1] Abbreviations: CNPG3, 2-chloro-4-nitrophenyl α-maltotrioside; 5FGlcF, 5-fluoro-α-D-glucosyl fluoride; 5FIdoF, 5-fluoro-β-L-idosyl fluoride; G3F, α-maltotriosyl fluoride; Glc, D-glucose; HPA, human pancreatic α-amylase; MeG2F, 4′-*O*-methyl-α-maltosyl fluoride; MPD, 2-methylpentane-2,4-diol; PPA, porcine pancreatic α-amylase. HPA amino acid numbering is according to the sequence alignment of ref *8*.

 Published on Web 10/05/2009

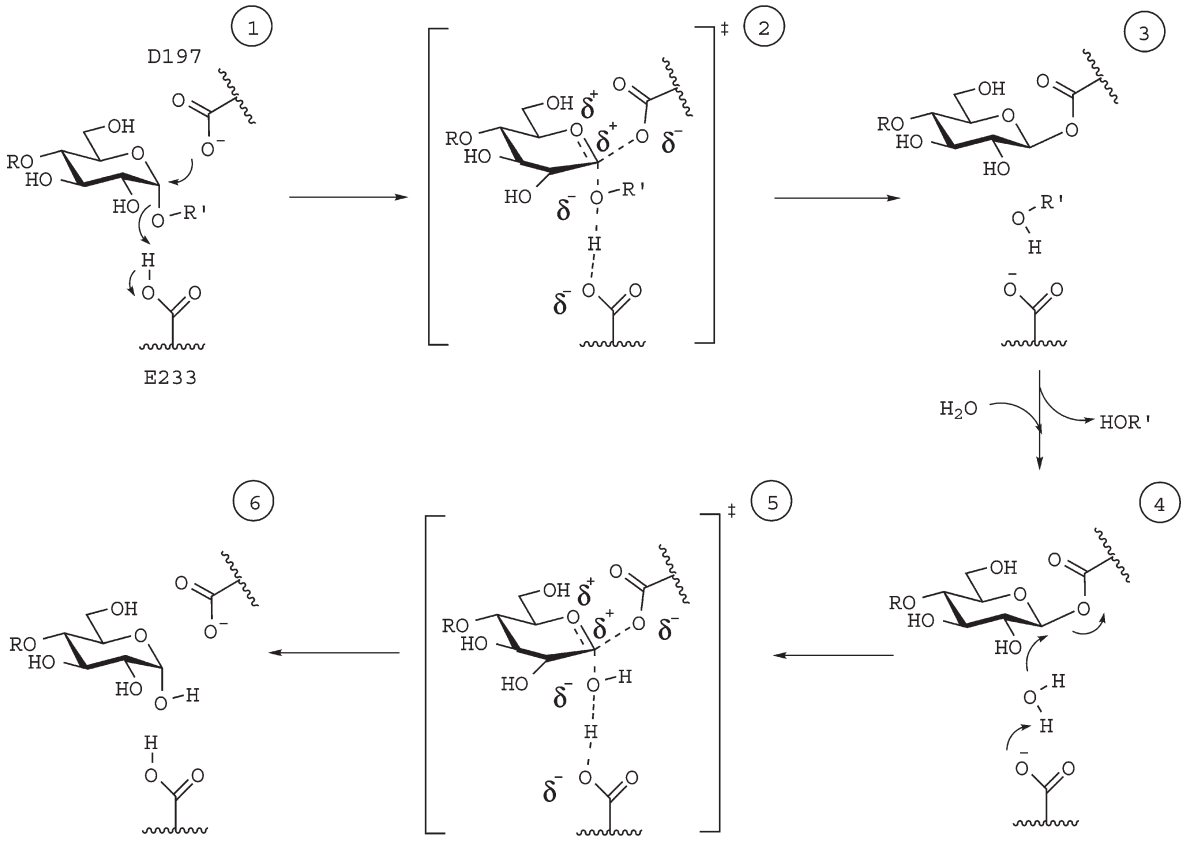

FIGURE 1: Proposed double displacement mechanism of α-amylases.

analyses of HPA confirm that these three residues (D197, E233, and D300) are located at the bottom of a "V"-shaped active site cleft in domain A (*12*, *15*). Amylases catalyze hydrolysis of glycosidic bonds with net retention of anomeric configuration via a classical double displacement mechanism (Figure 1) (*16*). The first part of the reaction sequence involves an acid-catalyzed nucleophilic displacement of the aglycon by a carboxylate residue at the active site (glycosylation step), leading to the formation of a covalent glycosyl-enzyme intermediate. In the second part of the reaction, this covalent intermediate is then hydrolyzed, with general base catalysis provided by the same group that earlier served as the acid catalyst (deglycosylation step). Overall, the reaction pathway proceeds through two oxocarbenium ion-like transition states. Previous kinetic studies strongly support a role for D197 as the catalytic nucleophile of HPA since mutation of this residue decreases enzymatic activity at least 10^6-fold (*12*, *15*). The identity of the general acid/base residue was somewhat less clear since both E233 and D300 were suitably poised for this role and replacement of either of these residues with the equivalent amide or alanine led to comparable decreases in enzymatic activity. However, pH profiles and the significantly greater second-order rate constant observed for E233 variants with "activated" substrates relative to the natural substrate starch are strongly suggestive of E233 filling the role of acid/base catalyst for HPA (*15*). Nonetheless, definitive evidence supporting this assignment remains elusive. Moreover, if E233 serves as the general acid/base residue, the role of D300 merits further clarification since it also plays an important role in catalysis.

The mechanistic questions surrounding HPA catalysis prompted us to design strategies to trap and then kinetically and structurally characterize the proposed covalent intermediate. This approach has the potential to provide unique insights into HPA function, especially with respect to the roles of the catalytic residues and anticipated sugar conformational distortions along the reaction coordinate (*17*−*19*). Structural studies of several trapped glycosyl-enzyme intermediates have been reported, the majority of these being with retaining β-glycosidases (*16*, *20*). Structures of trapped intermediates of α-glycosidases have proven more elusive, and of these the structures most relevant to the amylases are those of the GH13 cyclodextrin glucanotransferase from *Bacillus circulans* (*21*) and the amylosucrase from *Neisseria polysaccharea* (*22*). In each of these cases, the glycosyl-enzyme intermediate was trapped by mutation of their general acid/base residues to alanine or glutamine and incubating with a glycosyl fluoride substrate. In two other interesting cases, the covalent intermediate was unexpectedly trapped by incubating a crystal of either a GH77 amylomaltase (*23*) or a GH13 glycogen-debranching enzyme (*24*) with acarbose. Notably, in all cases, transglycosidases rather than glycosidases have been employed. To date, there has been no report of the structural analysis of a trapped covalent intermediate on a strictly hydrolytic α-amylase, despite considerable effort.

While trapping the covalent intermediates of transglycosidases has proven to be reasonably straightforward, simply deleting the acid/base residue is not a sufficient strategy for α-amylases, since they retain enough hydrolytic activity for turnover (*12*, *15*). An alternative trapping strategy is to utilize C2 or C5 fluorinated substrates possessing good anomeric leaving groups (*25*). The presence of a fluorine at C2 or C5 destabilizes the oxocarbenium ion-like transition states both inductively and (at C2) via the removal of key transition state-stabilizing interactions. As a consequence, both the formation and the turnover of the glycosyl-enzyme intermediate are slowed down. However, the incorporation of a good leaving group at the anomeric center,

such as fluoride or 2,4-dinitrophenolate, ensures that the intermediate is kinetically accessible and accumulates.

Generally, 2-deoxy-2-fluoroglycosides have proved to be effective agents for trapping intermediates on β-glycosidases, but these act as slow substrates for α-glycosidases, with the glycosylation step remaining rate-limiting (*12*). This problem can be overcome by incorporation of two fluorines at C2 to dramatically slow down both steps, in conjunction with the incorporation of a highly reactive trinitrophenolate leaving group at C1 to speed up glycosylation. While this strategy was successful in solution for HPA (*26*) and was definitively demonstrated for an α-galactosidase with the corresponding *galacto* analogue (*27*), crystallographic studies of this complex with HPA were thwarted by an unwanted nucleophilic aromatic substitution reaction with the aglycon (data not shown). Attempts were made to overcome this problem through the use of a chloride leaving group, but these were unfortunately unsuccessful (*28*). Another potential approach would be to use 5-fluoroglycosyl fluorides, which have worked well in trapping intermediates of other α-glycosidases (*29*, *30*). Application of this strategy to HPA would require the synthesis of a maltooligosaccharyl version of the 5-fluoroglycosyl fluorides, but the chemical synthesis of elongated 5-fluoroglycosyl fluorides has proven to be extremely challenging with only one report in the literature to date and that concerned disaccharides containing nonactivated anomeric leaving groups (*31*).

This paper describes the first detailed kinetic and structural characterization of a covalent glycosyl-enzyme intermediate of human pancreatic α-amylase, trapped using an oligosaccharyl 5-fluoro-L-idosyl fluoride synthesized *in situ* from the monosaccharide 5-fluoro-β-L-idosyl fluoride and an oligosaccharyl fluoride donor. These analyses provide new insights into the catalytic mechanisms of amylases, both in terms of the roles of active site residues and the conformational properties of covalently bound sugar residues at the site of cleavage.

MATERIALS AND METHODS

All chemicals and buffer salts, as well as porcine pancreatic α-amylase (PPA, EC 3.2.1.1, type I-A), were purchased from Sigma-Aldrich unless otherwise noted. HPA was purified according to literature procedures (*32*). 2-Chloro-4-nitrophenyl α-maltotrioside (CNPG3) was purchased from Genzyme Corp., Cambridge, MA. 5-Fluoro-α-D-glucosyl fluoride (5FGlcF), 5-fluoro-β-L-idosyl fluoride (5FIdoF), α-maltotriosyl fluoride (G3F), and 4′-*O*-methyl-α-maltosyl fluoride (MeG2F) were all synthesized as described previously (*29*, *33*).

General Assay Conditions. All kinetic studies were performed at 30 °C in 50 mM phosphate buffer containing 100 mM NaCl, pH 6.9, unless otherwise noted. Hydrolysis of CNPG3 by either HPA or PPA was monitored by the increase of absorbance at 400 nm using a Varian Cary 300 spectrophotometer equipped with a circulating water bath. Plastic cuvettes with a path length of 1 cm were used. All enzyme kinetic data were processed using the program GraFit 5.0.13 (Erithacus Software Limited, 2006).

Time-Dependent Inactivation Kinetics. Samples of HPA or PPA (0.32 μM) were incubated in buffer in the presence of a range of concentrations of both donor (20−40 mM MeG2F or G3F) and acceptor (25−50 mM 5FGlcF or 5FIdoF) at 30 °C. Aliquots (10 μL) of these inactivation mixtures were removed at time intervals and diluted into assay cells containing a large volume (1 mL) of CNPG3 substrate (2 mM) preincubated at 30 °C. This effectively stops the inactivation both by dilution of the inactivator and by competition with an excess of substrate. The residual enzymatic activity was determined from the rate of hydrolysis of the substrate, which is directly proportional to the amount of active enzyme.

Reactivation Kinetics. Fully inactivated HPA was freed of excessive inactivator by 10-fold dilution with buffer (500 μL) and then concentration at 4 °C using a 10 kDa nominal cutoff centrifugal concentrator to a volume of approximately 50 μL. This procedure was repeated a total of eight times. The resultant solution was then diluted to 200 μL either with buffer alone or with maltose solutions at different concentrations and then incubated at 30 °C. Reactivation was monitored by removal of aliquots (10 μL) at appropriate time intervals and assaying as described above.

Mass Spectrometry. Mass spectra were recorded using an ABI MDS-SCIEX API QSTAR Pulsar i mass spectrometer (Sciex, Thornhill, Ontario, Canada). Proteins were separated using a reverse-phase PLRP-S column on an Ultimate HPLC system (LC Packings, Amsterdam, The Netherlands) interfaced with the mass spectrometer. For LC/MS experiments, protein was loaded onto a PLRP-S column (Michrom BioResources, 75 μm i.d. × 50 mm) and eluted with a gradient of 15−60% solvent B in solvent A over the course of 20 min at a flow rate of 0.2 μL/min (solvent A, 0.05% TFA and 2% acetonitrile in water; solvent B, 0.065% TFA and 85% acetonitrile in water). The TOF mass analyzer was scanned over a mass-to-charge ratio range of 600−2200 amu, with a step size of 0.1 amu and a scan time of 1 s. The ion source potential was set at 2.4 kV; the orifice energy was 50 V.

Structural Determinations. Human pancreatic α-amylase was crystallized using the hanging drop vapor diffusion technique at a concentration of 10 mg/mL from 60% 2-methylpentane-2,4-diol (MPD) and 100 mM cacodylate at pH 7.5. Crystals with 5-fluoro-β-L-idosyl fluoride (5FIdoF) inhibitor bound to HPA in the presence of the elongation agents 4′-*O*-methyl-α-maltosyl fluoride (MeG2F) or α-maltotriosyl fluoride (G3F) were prepared under three conditions. In condition 1, an HPA crystal was soaked overnight in a solution containing 100 mM 5FIdoF, 60% MPD, and 100 mM cacodylate at pH 7.5. Subsequently, MeG2F was added to this solution to a final concentration of 150 mM, and the crystal was soaked in this combined mixture for a further 2 h. At this point the soaked HPA crystal was removed, mounted, and frozen in liquid nitrogen for data collection. A further experiment (condition 2) involved an overnight soak of an HPA crystal in a combined mixture of 100 mM 5FIdoF and 150 mM elongation agent G3F. Condition 3 soaking was similar to that of condition 1, except that the 5FIdoF and MeG2F components were both added at the beginning of the overnight soaking period and no additional MeG2F was added after this.

All diffraction data from HPA−inhibitor complexes were collected on an ADSC Q315R CCD detector at the Stanford Synchrotron Radiation Lightsource at 100 K and with an incident X-ray wavelength of 0.98 Å. Intensity data were integrated, scaled, and reduced to structure−factor amplitudes with the HKL software package (*34*). Observed space group and unit cell dimensions (Table 1) indicated that all HPA−inhibitor complex crystals were isomorphous with those of wild-type HPA (*8*, *32*, *35*). On this basis, the starting structural refinement model chosen for all inhibitor complexes was that of wild-type HPA. Refinement of structural models was accomplished with CNS (*36*), using alternating cycles of simulated annealing, positional and thermal factor *B* refinements. During this process, the

Table 1: Summary of Structure Determination Statistics

	complex structure[a]		
	MeG2F/5FIdoF/HPA (condition 1)	G3F/5FIdoF/HPA (condition 2)	MeG2F/5FIdoF/HPA (condition 3)
Data Collection Parameters			
space group	$P2_12_12_1$	$P2_12_12_1$	$P2_12_12_1$
unit cell dimensions			
a (Å)	52.0	52.4	52.1
b (Å)	68.5	68.0	67.8
c (Å)	129.9	130.0	129.9
no. of measurements	489089	229973	197577
no. of unique reflections	85356	40346	30917
mean $I/\sigma I$[b]	48.9 (10.1)	40.8 (9.3)	41.2 (11.6)
multiplicity[b]	5.7 (5.5)	5.7 (5.6)	6.4 (3.6)
merging *R*-factor (%)[b]	3.0 (16.5)	7.0 (15.1)	7.0 (19.4)
maximum resolution (Å)	1.43	1.85	2.0
Structure Refinement Values			
no. of reflections	85356	40346	30917
resolution range (Å)	50−1.43	33.4−1.85	50−2.0
completeness (%)[b]	98.8 (98.1)	99.7 (97.4)	96.9 (94.0)
no. of protein atoms	3946	3946	3946
no. of inhibitor atoms	51	49	59
no. of solvent atoms	406	307	231
average thermal factors (Å^2)			
protein atoms	18.8	19.7	19.7
inhibitor atoms	30.0	36.3	29.8
solvent atoms	32.8	30.9	26.7
final *R*-free value (%)[c]	21.3	20.7	22.9
final *R*-factor (%)	19.7	18.4	19.3
Structure Stereochemistry			
rmsd, bonds (Å)	0.005	0.006	0.006
rmsd, angles (deg)	1.01	1.02	0.99

[a]HPA crystal soaking procedures were as follows: condition 1, first in 100 mM 5FIdoF overnight and then 150 mM MeG2F solution for 2 h; condition 2, 100 mM 5FIdoF and 150 mM G3F overnight; condition 3, 100 mM 5FIdoF and 150 mM MeG2F overnight. [b]Values in parentheses refer to the highest resolution shell: 1.43−1.51 Å for the condition 1 complex, 1.85−2.03 Å for the condition 2 complex, and 2.0−2.07 Å for the condition 3 complex. [c]5% of the data was set aside to calculate *R*-free.

complete polypeptide chains for all three inhibitor complexes were examined periodically with $F_o - F_c$, $2F_o - F_c$, and composite omit electron density maps. Where necessary, manual model rebuilding was performed with O (*37*).

The location, composition, and preliminary placement of bound inhibitors in the three HPA−inhibitor complexes were readily apparent on the basis of difference electron density maps calculated during the refinement of the protein portion of these complexes. Following inhibitor placement in each complex, additional refinement of both the inhibitor (at full occupancy) and protein portions was carried out to convergence. As part of this process it was noted that, beyond inhibitor binding in the active site region in all three complexes, additional binding sites were observed for smaller inhibitor/substrate components at more remote locations. These included two 5FIdoF groups for condition 1 and 2 complexes and an MeG2F group for the condition 3 complex. Such remote binding sites have been observed in earlier studies of HPA complexes (*13*). For all structures, solvent peaks were identified in difference electron density maps, and the validity of these was monitored on the basis of hydrogen-bonding potential to protein and inhibitor atoms and the refinement of a thermal factor *B* of < 65 Å^2. Table 1 provides a summary of data collection, structural refinement, and polypeptide chain geometry statistics for all three structure determinations completed.

RESULTS AND DISCUSSION

Elongation Strategy and Kinetic Analyses. Our previous studies have shown that HPA is capable of generating a remarkably better reversible inhibitor by "*in situ*" elongation of a relatively poor inhibitor using activated glycosyl fluorides as donors, with the elongated inhibitor binding roughly 1000-fold tighter than the original species (*38*). On the basis of these observations, we hypothesized that either 5-fluoro-α-D-glucosyl fluoride (5FGlcF) or 5-fluoro-β-L-idosyl fluoride (5FIdoF) might also be elongated *in situ* by employing an appropriate glycosyl donor (MeG2F or G3F). In this method, the resultant elongated products might in turn act as high-affinity mechanism-based inhibitors and trap the proposed covalent intermediate in the active site of HPA (Figure 2). For this strategy to work, the activated oligosaccharyl fluoride donor must first bind to the −1 and −2 binding subsites and form a covalent intermediate with the enzyme. The 5FGlcF or 5FIdoF must then bind in the +1 binding subsite and react with this glycosyl-enzyme intermediate via transglycosylation to the 4-OH of the acceptor molecule. Since monosaccharide analogues generally have very weak

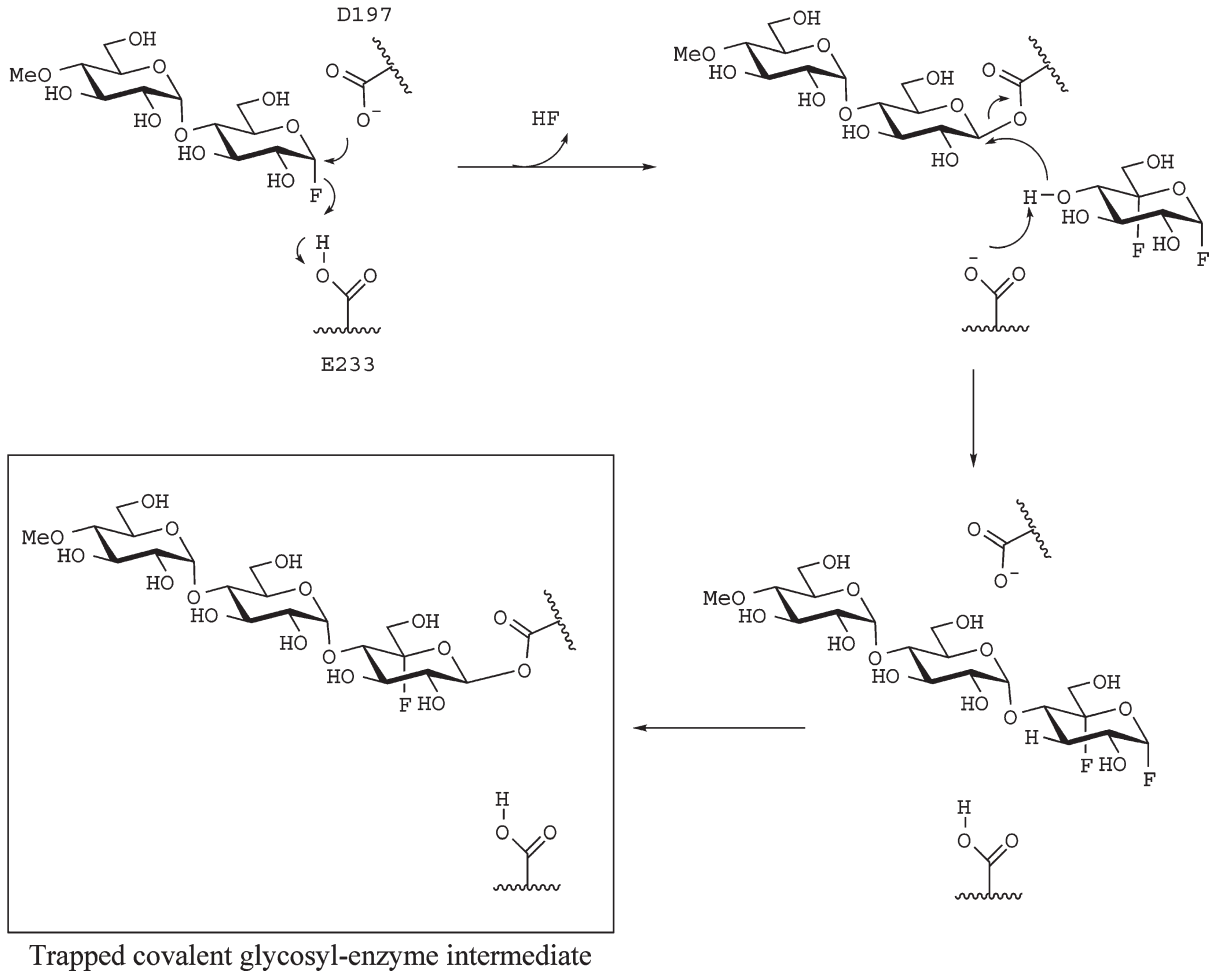

FIGURE 2: Proposed *in situ* elongation-trapping strategy using the example of 5FGlcF and MeG2F.

affinity for HPA's active site (*38*), high concentrations of 5FGlcF or 5FIdoF are required to optimize the chance of this occurring. The elongated inactivator formed would then need to disengage from the active site and rebind its 5-fluoro sugar moiety in the −1 subsite, followed by reaction with D197 to form the covalent intermediate of interest. The complication presented by self-transglycosylation of maltosyl or maltotriosyl fluoride donors to form a variety of elongated maltooligosaccharyl fluorides can be overcome by using a "capped" 4′-*O*-methylmaltosyl fluoride (MeG2F) as the donor.

Incubation of 50 mM 5FGlcF (acceptor) and 20 mM MeG2F (donor) with HPA at 30 °C did indeed result in a time-dependent loss of activity, such that less than 45% was left after 1 h of incubation (Figure 3). However, further incubation resulted in no further significant reduction of enzymatic activity. Instead, a "steady state" of residual activity was reached which lasted for ~2 h. Upon even more prolonged incubation enzymatic activity gradually recovered to that of the wild-type enzyme. This behavior is consistent with the "*in situ*" formation of an elongated inactivator, which then forms a transient intermediate that is slowly hydrolyzed. Notably, incubation of either 50 mM 5FGlcF (Figure 3) or 20 mM MeG2F alone (data not shown) with HPA resulted in no inactivation, clearly illustrating the need for formation of a reactive species via transglycosylation before inactivation can occur. This inability to obtain complete and long-term inactivation is reminiscent of previous studies with 5FGlcF and yeast α-glucosidase, where similar "steady-state" kinetic results were observed, due to

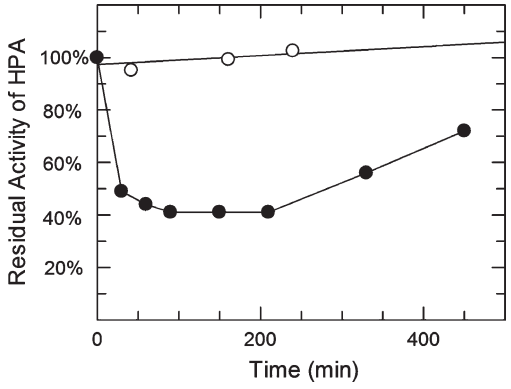

FIGURE 3: Residual activity of HPA in the presence of (○) 50 mM 5FGlcF and (●) 50 mM 5FGlcF + 20 mM MeG2F, at 30 °C.

relatively rapid inactivation and then reactivation by hydrolysis (*30*).

While these results with 5FGlcF were encouraging, the rapid turnover of the accumulated intermediate made a detailed examination of its structural characteristics problematic via X-ray crystallographic methods. A potential solution to this problem was suggested by kinetic studies on other α-glycosidases, which have shown that the C5 fluorinated substrate analogues with inverted configuration at C5 typically function as better mechanism-based inhibitors than their "natural" 5-fluoro counterparts, by forming longer lived glycosyl-enzyme intermediates (*30*, *39*). In the case of HPA, the utility of this approach

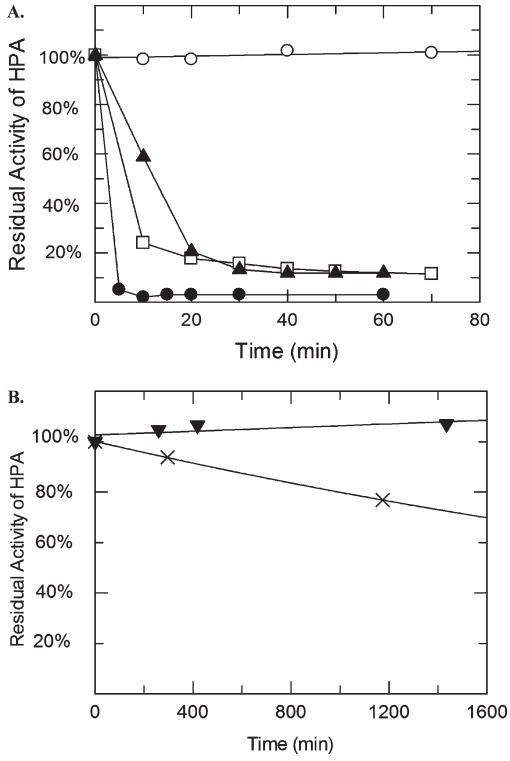

FIGURE 4: (A) Residual activity of HPA in the presence of (○) 50 mM 5FIdoF alone, (●) 50 mM 5FIdoF + 20 mM MeG2F, (□) 50 mM 5FIdoF + 40 mM MeG2F, and (▲) 25 mM 5FIdoF + 40 mM G3F, at 30 °C. (B) Long-term analysis of residual activity of HPA (▼) in the absence of any 5FIdoF and (×) in the presence of 100 mM 5FIdoF, at 30 °C. To prevent a change in pH during these experiments, higher concentrations of buffer salts (200 mM NaP_i, 100 mM NaCl) were used.

depended on whether the C5 epimer, 5FIdoF, could first act as an acceptor for transglycosylation and then, if so, whether it would react and form a long-lived intermediate.

As can be seen in Figure 4A, incubation of 50 mM 5FIdoF and 20 mM MeG2F with HPA at 30 °C resulted in rapid and essentially complete inactivation of HPA. Significantly, no recovery of activity was seen, even after prolonged (up to 6 h) incubation, suggesting that with elongated 5FIdoF a more stable covalent glycosyl-enzyme had been formed. Interestingly, when a higher concentration of the donor molecule (40 mM MeG2F) was used, inactivation was slower, presumably because MeG2F acts as a competitive inhibitor, "protecting" the active site of HPA from reaction with elongated 5FIdoF (Figure 4A). Even slower inactivation was observed when MeG2F was replaced by G3F, presumably because the elongated oligosaccharyl fluorides are even more effective "protecting agents". Again, control experiments revealed that either 20 mM MeG2F or 50 mM 5FIdoF alone had no impact on enzyme activity within 2 h, providing evidence that the elongated 5FIdoF generated *in situ* serves as the real inactivator. Interestingly, however, in longer term experiments in which HPA, either in solution or in the crystalline state (discussed later herein), was exposed to a very high concentration of 5FIdoF alone (100 mM or more), an extremely slow inactivation process was observed (Figure 4B).

Evidence for formation of an elongated covalent 5FIdoF species and insights into its composition were obtained using a mass spectrometry approach. Both the wild-type HPA and MeG2F-5FIdoF-treated HPA were analyzed by electrospray ionization mass spectrometry and individual masses determined

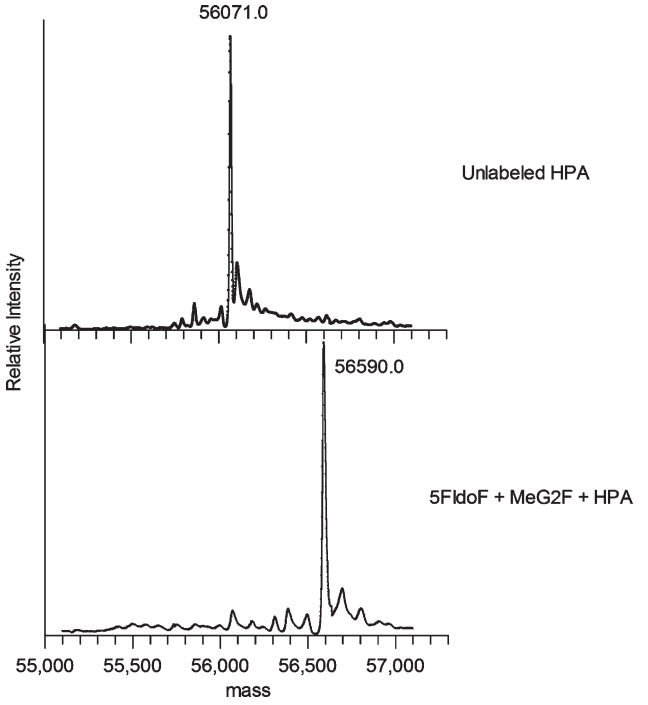

FIGURE 5: Mass spectra of HPA (above) and HPA treated with 25 mM 5FIdoF + 20 mM MeG2F (below).

to be 56071 and 56590 Da, respectively (Figure 5). The mass difference between these two species is 519 Da, which corresponds exactly with the molecular mass change (519 Da) due to the predicted covalent attachment of a trisaccharyl moiety containing a 5-fluoro-α-L-idosyl moiety at the reducing end. It is noteworthy that the mass spectra of the MeG2F-5FIdoF-treated HPA revealed essentially no free enzyme, indicating nearly complete covalent labeling, consistent with our kinetic results.

The catalytic competence of the trapped covalent intermediate could also be demonstrated by reactivation experiments, in which MeG2F-5FIdoF-treated HPA was first freed of excess inactivator and then incubated in buffer, and aliquots were assayed at time intervals. At 30 °C, reactivation was extremely slow with $k_{react} = (4.8 \pm 1.2) \times 10^{-5}$ min^{-1}, corresponding to a half-life of 240 h (Figure 6A). Since many glycosidases carry out transglycosylation more rapidly than hydrolysis (*40*), we investigated the effects of addition of maltose on reactivation rates. In these experiments, the presence of 20 mM maltose dramatically reduced the half-life of the trapped intermediate to 53 min. This observation opened up the possibility of measuring the binding affinity of maltose to the aglycon site of the glycosyl-enzyme intermediate of HPA. This could be done in a direct manner by measuring the rates of reactivation at different concentrations of maltose and then plotting the apparent reactivation rate constants as a function of maltose concentration (see Figure 6B). From this work a dissociation constant for maltose of $K_d = 69 \pm 17$ mM and a maximal reactivation rate constant of $k_{react} = 0.073 \pm 0.008$ min^{-1}, corresponding to a half-life of 10 min, were determined (Figure 6C).

To determine the generality of this elongation approach to the study of covalent intermediates of α-amylases, we carried out a comparable series of experiments with porcine pancreatic α-amylase (PPA) (*41*, *42*). When both the donor (25 mM 5FIdoF) and acceptor (20 mM MeG2F) were incubated with PPA, very fast inactivation was seen, with essentially no enzymatic activity left

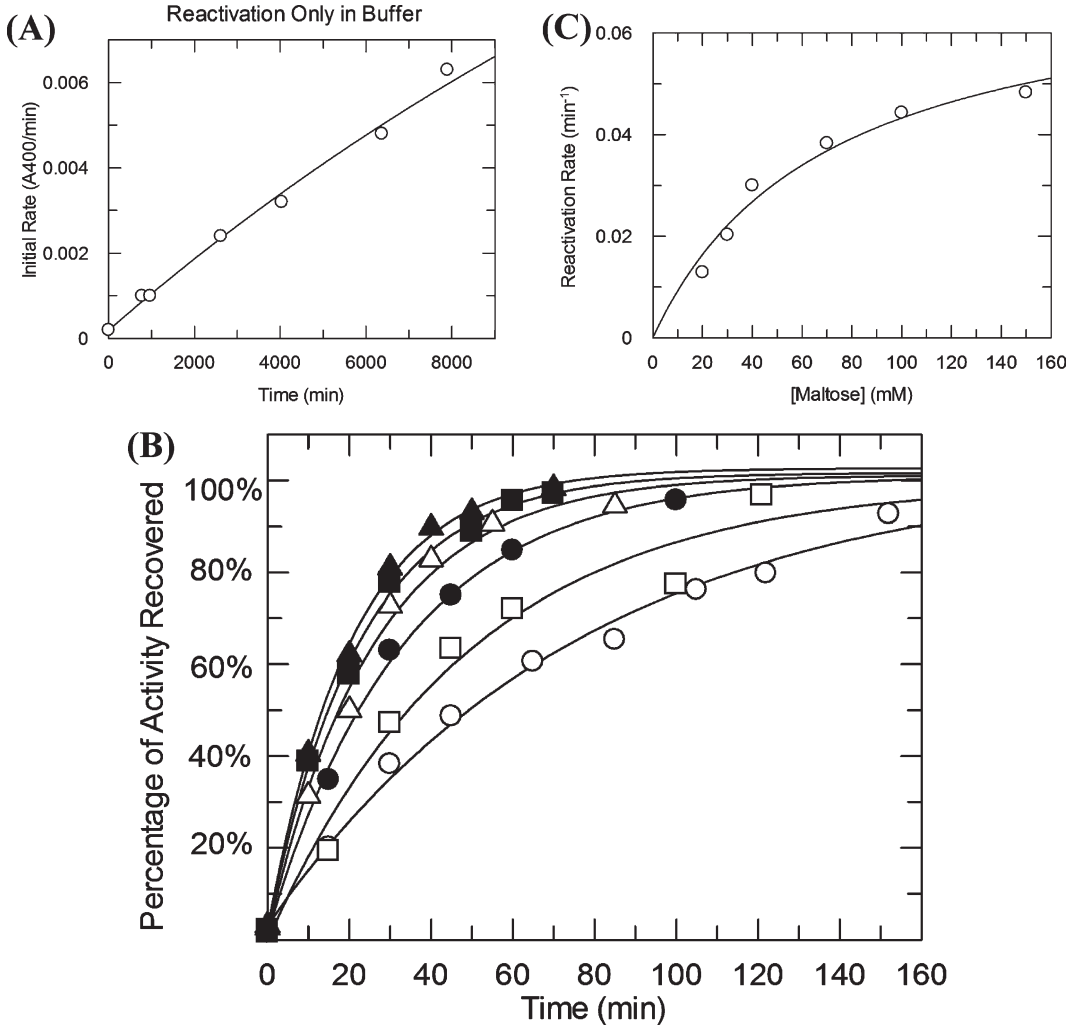

FIGURE 6: Reactivation of inactivated HPA at 30 °C in the presence of (A) only buffer and (B) different concentrations of maltose: (○) 20 mM maltose; (□) 30 mM maltose; (●) 40 mM maltose; (Δ) 70 mM maltose (■); 100 mM maltose; (▲) 150 mM maltose. Lines represent fits to first-order expressions, yielding apparent first-order rate constants for reactivation at each concentration. A replot of these apparent reactivation rate constants as a function of maltose concentration, fitted to the Michaelis−Menten equation, is shown in frame C.

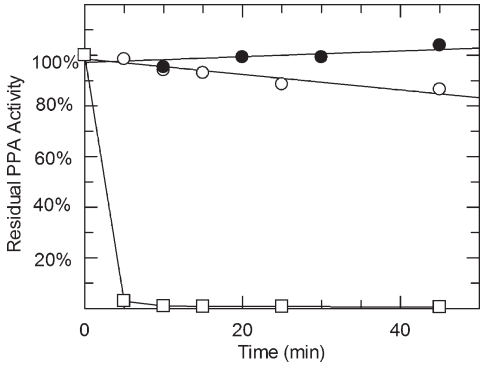

FIGURE 7: Residual activity of porcine pancreatic α-amylase in the presence of (●) 20 mM MeG2F, (○) 25 mM 5FIdoF, and (□) 20 mM MeG2F + 25 mM 5FIdoF, at 30 °C.

after 10 min (Figure 7). As expected, incubation of 20 mM MeG2F (donor) alone with PPA results in no time-dependent inhibition. Interestingly, incubation of 25 mM 5FIdoF (acceptor) alone with PPA yielded a very slow, but detectable loss of enzymatic activity, with this process being much faster than that observed for HPA (Figure 4). This faster inactivation of PPA may indicate a broader specificity of PPA for binding and turnover of the 5FIdoF monosaccharide in the −1 binding subsite than is the case with HPA. Most importantly, this observation of greatly enhanced inactivation of both PPA and HPA in the presence of 5FIdoF and MeG2F illustrates the generality of this *in situ* elongation strategy for the study of covalent intermediates in α-amylases and quite likely other retaining endoglycosidases.

Structure of the Monosaccharide 5-Fluoroidosyl-HPA (Condition 1) Complex. Excellent high-resolution diffraction data (1.43 Å) were obtained from an HPA crystal initially soaked in a solution of 100 mM 5FIdoF overnight, after which 150 mM MeG2F was added for an additional 2 h (Table 1). Strong continuous electron density in subsequent electron density maps clearly demonstrated the covalent attachment of a monosaccharide 5-fluoroidosyl moiety to the side chain OD1 oxygen atom of the putative active site nucleophile D197 (Figure 8). In forming this covalent bond the anomeric fluoride of 5FIdoF has been displaced and replaced by the side chain of D197, with inversion of anomeric configuration, as expected. The identity of the bound 5-fluoro-L-idosyl intermediate was further confirmed by the observation of the fluorine atom at C5 and the axial orientation of the C-6 CH_2OH substituent.

Notably, in these structural studies only the single sugar moiety derived from 5FIdoF is found covalently bound to

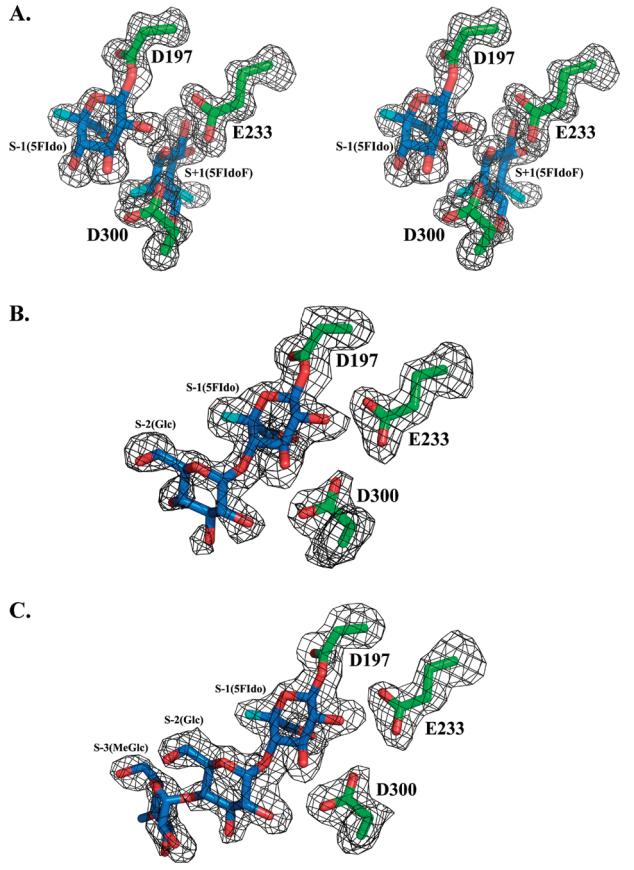

FIGURE 8: Omit difference electron density maps of the (A) monosaccharide 5-fluoroidosyl-HPA (condition 1), (B) G3F/5FIdoF (condition 2), and (C) MeG2F/5FIdoF (condition 3) covalent glycosyl-intermediate complexes bound in the active site of HPA. Note that frame A is drawn as a stereo diagram to more clearly show both the bound covalent intermediate and the associated noncovalently bound 5FIdoF moiety in the +1 binding subsite. All of these difference electron density maps were calculated with the intermediates and the side chains of D197, E233, and D300 omitted. Difference electron density contours have been drawn at the 2.8 σ level and overlaid with the final refined structures of each intermediate complex (blue backbone) and the side chains of the omitted residues (green backbone). The identity of each individual sugar ring has been indicated along with the binding subsite in which it resides (also see Figure 9).

D197 in the active site (at full occupancy) with no evidence of further elongation by MeG2F in electron density maps. Clearly, overnight exposure to high concentrations (100 mM) of 5FIdoF leads to complete inactivation of HPA and negates the ability of the enzyme to elongate this inhibitor upon subsequent incubation with MeG2F. This is consistent with the results of kinetic studies, which indicate that 5FIdoF, by itself, will slowly inactivate HPA and that the covalent intermediate formed is stable (Figure 4). As will be discussed later, quite different results are obtained when crystals are soaked simultaneously in a combined 5FIdoF and MeG2F solution (see condition 3 results) to give a covalent complex that consists entirely of elongated intermediate. Our results also demonstrate the apparent inability of 5FIdoF to elongate via transglycosylation with itself.

As is evident in the electron density map for this complex in Figure 8 and the resultant schematic representation in Figure 9, the covalently attached 5FIdo ring is bound in a $^4C_1$ chair conformation and is positioned in the −1 binding subsite, attached to the side chain of D197. This correlates well with the expected bound conformation of a glucose residue at this site in a normal polymeric starch substrate (Figure 9). However, binding in this conformation might at first seem surprising for the analogue in question since L-idosyl rings, and especially 5-fluoro-L-idosyl rings, are substantially distorted in solution in order to avoid the steric repulsions associated with an axial hydroxymethyl group at C-5 and in order to maximize anomeric effects associated with an electronegative "anomeric" substituent at C-5 (*30*). As is apparent from the structure, a relatively large cavity exists on the α-face of the sugar that can accommodate the bulky axial CH_2OH substituent of the 5-fluoroidosyl moiety, making such binding possible. In addition, since the hydrogen-bonding interactions at the active site have been optimized for binding of a sugar in a $^4C_1$ conformation, the enzyme will stabilize the sugar in this conformation. A very similar result was seen in the structure of another α-glycosidase for which a trapped 5-fluoroglycosyl-enzyme intermediate has been described, that being an α-mannosidase (*39*). In that example, the 5-fluoro-L-gulosyl-enzyme intermediate adopted exactly the same ($^1S_5$) conformation as a 2-fluoro-D-mannosyl-enzyme intermediate trapped on the same enzyme, showing that a bulky epimeric substituent at C5 could be accommodated. Indeed, in that case a large protein cavity was also observed on the back face of the sugar. Presumably such space is necessary to accommodate the conformational changes occurring within the sugar ring along the reaction coordinate.

Satisfyingly, the side chain carbonyl oxygen of D197 in this covalent complex has as its nearest neighbor (2.7 Å) the endocyclic oxygen of the covalently attached 5-fluoroidosyl moiety. This is exactly what was seen in the three-dimensional structures of trapped covalent intermediates in CGTase (*21*) and Golgi α-mannosidase II (*39*). The suggestion was made that such an O−O interaction would serve to destabilize the "ground state" structure of the covalent intermediate but that, upon transition state formation, the relative positive charge formed on the endocyclic oxygen would reduce this unfavorable interaction, thereby contributing to relative transition state stabilization. A similar mechanistic strategy therefore seems to be in play in HPA.

Beyond the covalent bond made to D197, several hydrogen-bonding interactions with other 5FIdo ring substituents are seen (Figure 10A). For example, the conserved side chain of the active site residue D300 forms two strong hydrogen bonds to the C2 and C3 hydroxyls of the 5FIdo ring, serving to confirm the key role played by this residue in orienting intermediates within the −1 binding subsite (*15*). Interestingly, the side chain of D300 also binds a water molecule, in concert with the side chain of E233, the acid/base catalyst in the proposed reaction scheme (Figure 1). Indeed, E233 is ideally poised to carry out this function in the structure determined here. Other important interactions include hydrogen bonds to the side chains of H201, H299, and R195. The involvement of the side chain of R195 is of particular interest as it forms a bridging interaction between the side chain of E233 and the "ester-type" oxygen atom of D197 that forms the covalent bond to the 5-fluoroidosyl moiety. The importance of R195 to catalysis has been demonstrated by the 450-fold reduction in rate observed upon mutation (*9*). Notably, this residue is itself influenced by direct interactions with a bound chloride ion that has been shown to be important for efficient catalytic activity (*10*, *11*). This more remotely bound anion resides in a well-defined binding pocket off to one side of the active site cleft, where it also forms an important interaction with E233.

An unexpected finding of this structural determination was the observation of a second, noncovalently bound, 5FIdoF ring in

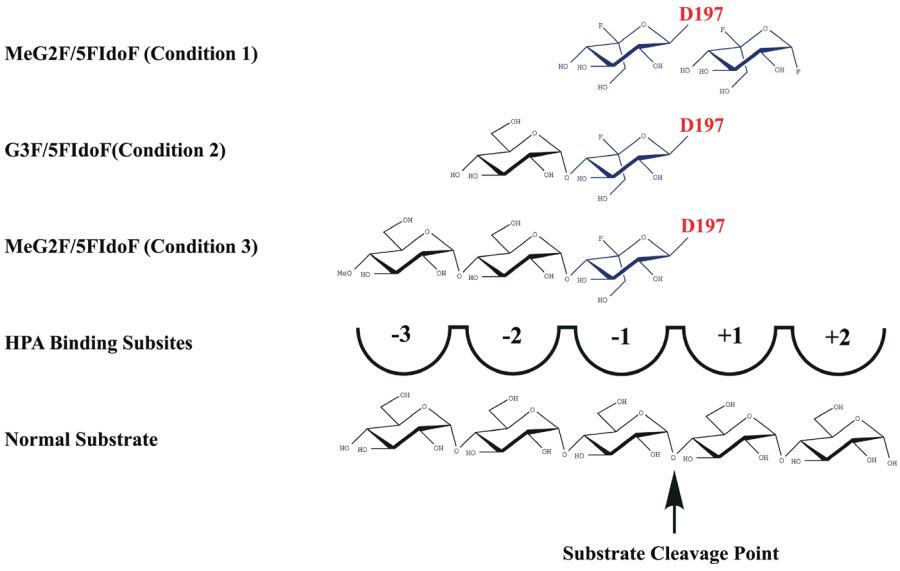

FIGURE 9: Schematic drawings of the structures determined for the condition 1−3 covalent glycosyl-intermediate complexes in the active site of HPA. Unique to the condition 1 structure is a noncovalently bound 5FIdoF moiety in the +1 binding subsite. Well-defined, high-affinity binding subsites in the active site cleft of HPA have been identified according to the convention indicated in the lower portion of this diagram (*15*, *32*). Also shown is the expected binding mode for a normal starch substrate, where hydrolysis would occur between subsites −1 and +1.

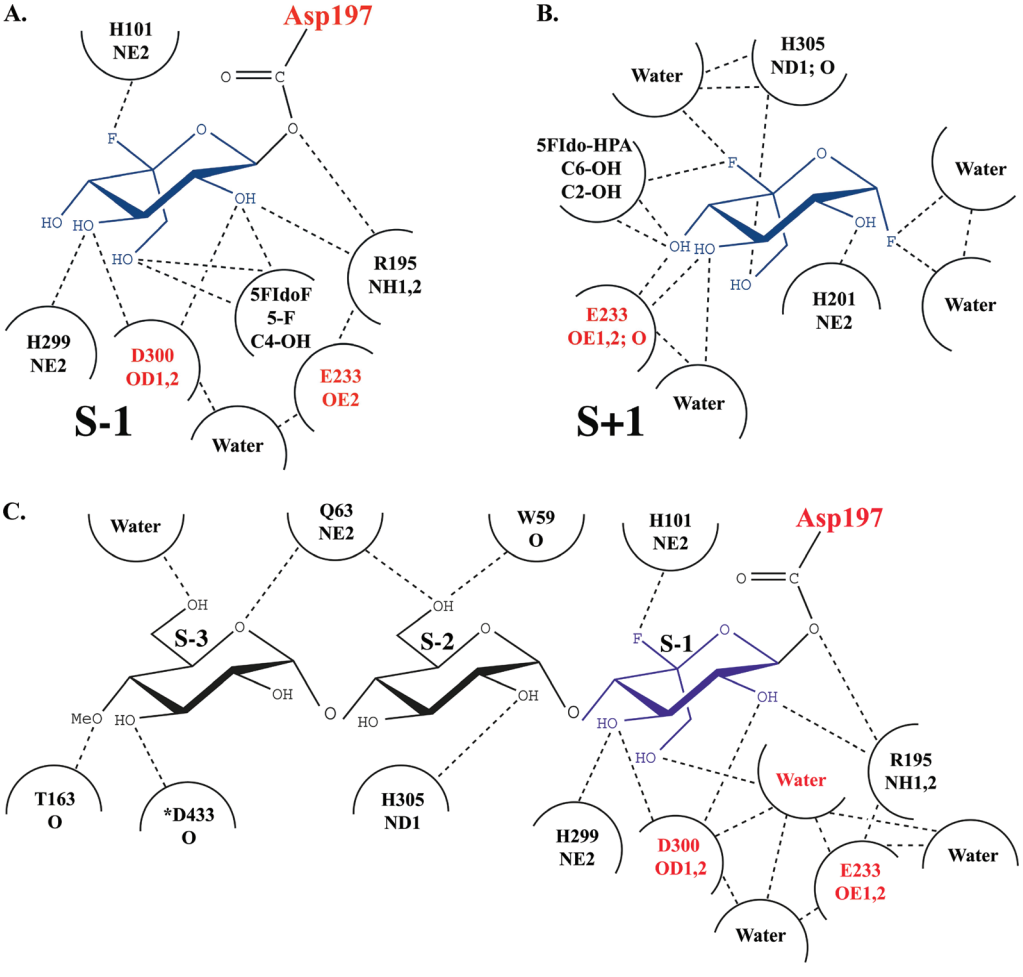

FIGURE 10: Schematic diagrams illustrating the hydrogen-bonding interactions formed in the active site of HPA in the (A) −1 binding subsite (covalent portion) and (B) the +1 binding subsite (noncovalent portion) of the MeG2F/5FIdoF (condition 1) glycosyl-enzyme intermediate complex. In (C) the hydrogen-bonding interactions for the elongated MeG2F/5FIdoF (condition 3) covalent glycosyl-enzyme intermediate complex are indicated. The 5FIdo moieties are drawn in blue, while catalytic residues are shown in red. The subsites of HPA occupied by each bound sugar moiety are indicated, and interacting amino acids are designated with their one-letter codes and sequence numbers.

the +1 binding subsite of the active site binding cleft (Figure 9). This moiety is also well-defined (Figure 8) and present at full occupancy. As is evident in Figure 9, this 5FIdoF group is positioned where one would normally expect the first product to

reside during a hydrolytic cycle, preceding its expulsion off the surface of the enzyme (Figure 1). Furthermore, like the expected normal product, the 5FIdoF ring binds such that only 3.7 Å separates its C4-OH and the C1 carbon of the covalently bound 5FIdo ring. A number of additional stabilizing interactions are made to the ring substituents of the noncovalently bound 5FIdoF, including hydrogen bonds from the side chains of H201, H305, and the catalytic residue E233 (Figure 10B).

The surprising presence of 5FIdoF in the +1 binding subsite, is likely due, in part, to the high concentration of this inhibitor present under the experimental conditions used for structural studies and its structural similarity to glucose, which would normally occupy this subsite. However, hydrogen bond interactions present between the covalently and noncovalently bound 5FIdoF groups may also be important. Indeed, these interactions may be mutually beneficial in the initial binding of both moieties of 5FIdoF in their respective binding subsites and may facilitate the formation of the monosaccharide covalent intermediate observed. These interactions include hydrogen bonds from the axial C6-CH_2OH of the covalently linked sugar to the C5-F (2.7 Å) and C4-OH (2.7 Å) groups of the noncovalently bound inhibitor. The normal orientation of the C6-CH_2OH group in a starch substrate would preclude such an interaction. Interestingly, the C6-CH_2OH group of the noncovalently bound 5FIdoF inhibitor is directed out toward solvent and, thus, does not disrupt binding in the +1 binding subsite. Also notable is the close interaction (2.7 Å) formed between the C2-OH of the covalently bound 5FIdo ring and the C4-OH of its noncovalently bound counterpart. This interaction would be possible for normal substrates and could constitute an important transition state stabilizing interaction with the first product of the reaction pathway as it leaves the enzyme surface (Figure 1). Equivalently, this interaction might also serve to stabilize the transition state in the transglycosylation mode of the reaction pathway.

Two additional 5FIdoF moieties are found bound to HPA, but at remote locations on the enzyme surface that are far too distant to influence binding in the active site region. The existence of such remote binding sites on HPA has been noted before (*13*, *38*), and the suggestion has been made that such sites may be involved in starch binding, but no definitive proof has been obtained.

It is instructive to compare the structure of the 5-fluoroidosyl-enzyme intermediate with noncovalent complexes such as that formed by acarbose (Figure 11A). The small shifts observed in catalytic residues and the active site as a whole, between the wild-type and the 5FIdoF and acarbose complexed structures, clearly suggest the relative rigidity with which the enzyme surface is held and the key role that substrate conformational flexibility must play in catalysis. Among the enzyme movements observed is a small shift in the highly mobile residues 301−308, which reside along one side of the active site cleft. This readjustment in polypeptide chain serves to optimize inhibitor−enzyme interactions, primarily in more remote binding subsites (*12*, *15*). Also observed is the reorientation of the plane of the side chain of Y62, which rotates so as to track orientational changes in the ring bound in the −1 binding subsite. This is shown in Figure 11A and presumably serves to contribute to both binding affinity and the proper orientation of substrate adjacent to the point of cleavage.

Taken together, the 5FIdoF and acarbose complexes provide insights into the conformational changes occurring in the substrate on going from a noncovalent intermediate complex through to covalent intermediate formation with D197. As can be seen in Figure 11A, the conformational changes would appear

A. Monosaccharide 5FIdoF (Condition 1)/ Acarbose Overlay

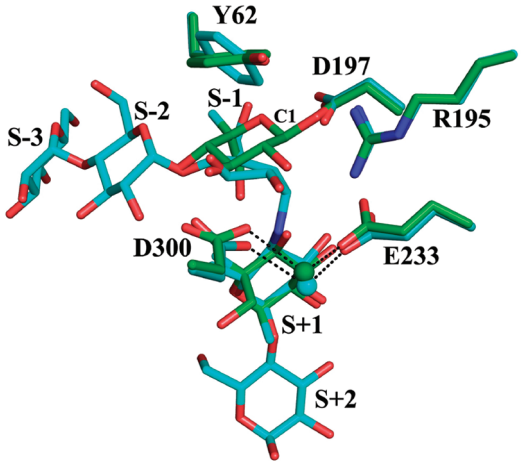

B. Trisaccharide 5FIdoF (Condition 3)/ Acarbose Overlay

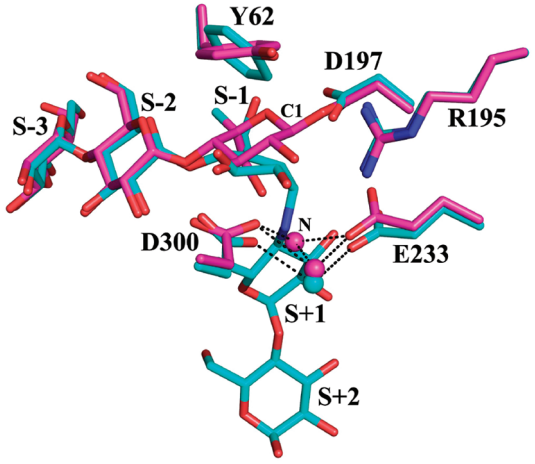

FIGURE 11: Overlays of the bound structures of the (A) monosaccharide 5-fluoroidosyl-HPA (condition 1) intermediate in green and the (B) MeG2-5FIdo-HPA (condition 3) intermediate in magenta, on top of the structure found for the noncovalent transition state mimic acarbose in cyan, in the active site of HPA adjacent to catalytic residues.

to be largely limited to the ring bound in the −1 binding subsite and primarily involve the C2, C1, O5, and C5 ring atoms, with the largest displacements involving the C1 and C5 atoms (~2.2 Å). Interestingly, the nitrogen atom of acarbose lines up almost exactly with the C4-OH of the first product mimic represented by the noncovalently bound 5FIdoF in the +1 binding subsite, suggesting that the +1 binding subsite portion of a substrate undergoes relatively little reorientation during the formation of the covalent intermediate.

Structure of the Disaccharide G3F/5FIdoF/HPA (Condition 2) Complex. In a second approach, we soaked a crystal of HPA in a solution containing both 100 mM 5FIdoF and 150 mM G3F overnight before collecting X-ray diffraction data (Table 1). In subsequent electron density maps, strong contiguous electron density confirmed both a covalent linkage between a bound 5FIdo ring and the side chain of D197 and the elongation of this intermediate by one glucose unit (Figures 8 and 9). As observed for the monosaccharide 5FIdoF complex, the sugar is attached to D197 through an equatorial linkage. The identities of the two sugar rings present were confirmed by the L-configuration and the presence of the C-5 fluorine in the case of

the 5FIdo ring and the absence of these features for the glucose unit. This elongated intermediate was found to be bound at full occupancy.

Based on the composition of the disaccharide intermediate observed, it is clear that both transglycosylation and hydrolysis reactions have played a role in converting the initial mix of 5FIdoF and G3F to the final product (*12*, *13*). Based on earlier studies of the preferred substrate cleavage patterns of HPA, a number of hydrolysis/transglycosylation routes are possible in this case. Most likely is the transglycosylation of a maltotriosyl unit from G3F on to 5FIdoF to form a tetrasaccharide, followed by the hydrolysis of the terminal maltose to yield Glc-5FIdoF, which could then react to form the covalent intermediate, blocking the active site.

Interestingly, the two additional 5FIdoF moieties found remotely bound outside the active site region in the monosaccharide covalent intermediate are also observed bound in similar conformations in the disaccharide complex. This indicates that a substantial concentration of free 5FIdoF remains at the end of the various hydrolysis/transglycosylation reactions that occur in the active site. In view of this result and given its initially higher concentration in the crystal soaking mixture, it would seem that much of the G3F originally present is involved in self-transglycosylation and hydrolysis reactions, which would ultimately be expected to result in maltose. It is also clear from Figure 4 that these various G3F products act as competitive inhibitors of 5FIdoF elongation and subsequent covalent intermediate complex formation. These conclusions are supported by the absence of 5FIdoF binding at remote binding sites when a nontransglycosylatable substrate such as MeG2F is used as the elongation agent, as will be discussed later.

In contrast to what is seen in the monosaccharide covalent intermediate complex, no 5FIdoF is seen in the +1 subsite in the disaccharide intermediate (Figures 9 and 12). Instead, a new water molecule has been substituted and positioned comparably to the C4-OH of the replaced 5FIdoF. Given the similarity of covalent intermediate attachment to D197 and the evident availability of free 5FIdoF in the soaking solution, as apparent from the observation of this group bound at remote surface sites, the origin of this difference at the +1 binding subsite must lie in subtle conformational displacements. Indeed, a comparison of the mono- and disaccharide covalent intermediates (Figure 12) shows that the C6-CH_2OH of the covalently bound 5FIdo ring in the monosaccharide complex, which hydrogen bonds with the C5-F and C4-OH groups of the 5FIdoF bound in the +1 binding subsite, is slightly reoriented in the disaccharide complex. This displacement appears to be a consequence of the elongated nature of the disaccharide covalent intermediate, which places additional conformational restraints on the C6-CH_2OH group of the 5FIdo ring. As will be discussed later, a similar, but even more pronounced C6-CH_2OH shift is observed in the additionally elongated trisaccharide covalent intermediate structure.

As can be seen in Figure 12, the conformation of the 5-fluoroidosyl moiety is the same in the mono- and disaccharide covalent intermediates as are the hydrogen bond interactions present in the −1 binding subsite (Figure 10). Furthermore, no appreciable shifts are observed in the active site residues D197, E233, D300, or R195. Also present, although slightly shifted, is a water molecule jointly bound between D300 and E233, which had been identified in earlier studies as potentially playing a role in catalysis (*15*). Our current studies suggest that a new water molecule in the disaccharide complex (labeled "N" in Figure 12),

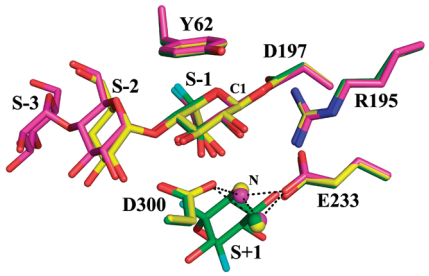

FIGURE 12: A comparative overlap of the structures of the covalently bound monosaccharide 5-fluoroidosyl-HPA (condition 1) intermediate in green, the G3F/5FIdoF (condition 2) intermediate in yellow, and the MeG2F/5FIdoF (condition 3) intermediate in magenta. Active site residues are color coded to correspond to the bound intermediates, and binding subsites for individual sugar residues are indicated (see also Figure 9). Water molecules bound between E233 and D300 have been drawn and color coded. Although related hydrogen-bonding interactions are observed for these water molecules in all three intermediate complexes, for clarity only those for the MeG2F/5FIdoF (condition 3) structure are drawn. The water molecule (labeled "N") located closest to the C1 carbon of the 5FIdo residue in the −1 binding subsite would be expected to act as the nucleophile in the next step of catalysis.

which is positioned much closer to the C1 carbon atom of the covalent intermediate, would seem to be more representative of a nucleophilic water. It is striking that this water molecule is located nearly identically to both the C4-OH of the +1 binding subsite 5FIdoF of the monosaccharide intermediate and the inter-ring nitrogen in the complex formed by acarbose. From this position, this water molecule is ideally poised, from both the perspective of distance and trajectory, to proceed with nucleophilic attack on the C1 carbon of the covalent intermediate formed with D197 and at the same time donate a proton to the side chain of E233, the acid/base catalyst. As such, the disaccharide complex structure observed would appear to be an excellent representative of step 4 in the reaction pathway (Figure 1).

Structure of the Trisaccharide MeG2F/5FIdoF/HPA (*Condition 3*) *Complex*. To achieve greater control over the elongation process for kinetic and structural studies and extend the length of the covalent intermediate into the −3 subsite, the capped oligosaccharyl fluoride donor MeG2F was employed in further studies. To this end a crystal of HPA was soaked in a solution containing both 100 mM 5FIdoF and 150 mM MeG2F overnight. Following the collection of diffraction data (Table 1), calculated electron density maps clearly illustrated the covalent nature of binding to the side chain of D197 and the fact that the bound intermediate included a total of three sugar rings. As observed for the mono- and disaccharide complexes already discussed, the ring directly attached to D197 could be definitively identified as a 5-fluoroidosyl moiety. Furthermore, the rings bound in the more distant −2 and −3 binding subsites could also be clearly identified as glucose residues (Figure 8), consistent with transglycosylation of a 4′-*O*-methylmaltosyl moiety onto 5FIdoF to give the Me-Glc-Glc-5FIdoF inactivator, which then forms the trapped intermediate. Interestingly, even though mass spectrometry confirmed the structure of the intermediate (Figure 5), the *O*-methyl substituent could not be seen in electron density maps, likely due to motional disorder. This has proven to be a consistent observation in structural studies wherein MeG2F has been used as an elongation reagent (*13*, *38*).

As illustrated in Figure 10, the trisaccharide covalent intermediate forms extensive hydrogen-bonding interactions with the

enzyme surface, with many of these involving the extended intermediate in the −2 and −3 binding subsites. As with the mono- and disaccharide complexes, the 5FIdo ring is well resolved and present at full occupancy. Attesting to the affinity of the additional interactions present in the −3 binding subsite, the glucose unit in the −2 binding subsite is better resolved and somewhat shifted from its position in the disaccharide intermediate (Figure 12). Notably, both the di- and trisaccharide intermediates share a small reorientation of the C6-CH_2OH group of the covalently bound 5FIdo ring in comparison to the monosaccharide intermediate, accounting for the finding that neither of these complexes contains an additional 5FIdoF group in the +1 binding site. Also in common is the new water molecule in the +1 binding site that would appear to be appropriately positioned to act as the nucleophilic water (labeled "N" in Figure 11).

Interestingly, the two remotely bound 5FIdoF moieties found outside the active site region in the mono- and disaccharide intermediate complexes are absent in the trisaccharide complex structure. Instead, a single MeG2F is found bound to the enzyme surface at an alternate remote binding site. Previous studies utilizing MeG2F as an elongation agent have also demonstrated binding at this site, the role of which would appear to relate to the initial global positioning of large-scale polymeric substrates such as starch, adjacent to HPA (*13*).

This latter, trisaccharyl-enzyme intermediate structure provides the best view of the covalent intermediate formed on HPA, since all three sugars are highly resolved and the nucleophilic water molecule is even clearly seen. It is particularly interesting to note that all three sugars are bound in a $^4C_1$ conformation, despite the considerable potential for distortion imposed by the axial hydroxymethyl group and equatorial fluorine at C5 on the sugar in the −1 subsite. Clearly, interactions with the enzyme are strongly stabilizing this otherwise unfavorable conformation, much as was seen in an equivalent case with the Golgi α-mannosidase II intermediate structures (*39*). This strongly suggests that HPA, and presumably other GH13 amylases, stabilizes the intermediates in the normal $^4C_1$ (chair) conformation. This has raised concerns since a distorted conformation that optimizes in-line attack by minimizing 1,3-diaxial-like repulsive interactions between the incoming water and H-3 and H-5 had been expected for retaining α-glucosidases, much as has been seen for bound substrates with β-glucosidases (*17*, *18*). While the intermediates formed on transglycosidases from GH13 had already been seen to adopt the $^4C_1$ conformation (*21*, *22*), it was suggested that this could be a mechanism for increasing the lifetime of the intermediate to allow time for the leaving group to diffuse out of the active site and the acceptor group to enter the +1 subsite (*19*). Such was not expected for the hydrolytic amylases. While undoubtedly a distorted conformation must be formed at the transition state, as also evidenced by the tight binding of acarbose, possibly the need for significant distortion within the covalent intermediate has been overrated. The β-configured acylal intermediate is quite inherently reactive and appears to be further destabilized electronically by the interaction of the endocyclic oxygen with the side chain carbonyl oxygen of D197. This may provide sufficient activation to drive efficient hydrolytic cleavage (*43*).

CONCLUSIONS

Although the requirement for a covalent catalytic intermediate has been hypothesized for hydrolysis reactions involving α-amylases, the structural characterization of such intermediates has been elusive since the necessary oligosaccharide-based reagents for trapping the intermediate have proven to be synthetically challenging. Nonetheless, by combining the activated monosaccharide 5FIdoF with the intrinsic ability of HPA to catalyze transglycosylations, it has been possible to elongate monosaccharide analogues of this type by incubation with activated substrates such as G3F and MeG2F. This "*in situ*" elongation approach greatly accelerates covalent intermediate formation, and the prolonged stability of the MeG2-5FIdo-HPA complex has allowed its detailed structural characterization in the active site of HPA under a number of conditions. Somewhat surprisingly the sugar in the −1 subsite adopts a clear $^4C_1$ conformation, counter to expectations, suggesting that the intermediate formed is sufficiently reactive for efficient hydrolysis without the need for conformational activation. Kinetic and structural data of this type provide an invaluable backdrop for the development of novel inhibitors of HPA, an important pharmaceutical target for the control of blood glucose levels in patients with indications for diabetes or obesity. The generality of our elongation approach allows for its application to other α-amylases of mechanistic or medical interest and quite probably to retaining endoglycosidases of other types.

ACKNOWLEDGMENT

We thank Robert Maurus for helpful discussions regarding structural analyses. S.G.W. thanks the Canada Research Chairs program for salary support and the Canada Foundation for Innovation and the B.C. Knowledge Development fund for support of infrastructure used. Portions of this research were carried out at the Stanford Synchrotron Radiation Lightsource, a national user facility operated by Stanford University on behalf of the U.S. Department of Energy, Office of Basic Energy Sciences. The SSRL Structural Molecular Biology Program is supported by the Department of Energy, Office of Biological and Environmental Research, and by the National Institutes of Health, National Center for Research Resources, Biomedical Technology Program, and the National Institute of General Medical Sciences. The graphics program PyMOL (*44*) was used in part to generate Figures 8, 11, and 12.

REFERENCES

1. Berman, H. M., Westbrook, J., Feng, Z., Gilliland, G., Bhat, T. N., Weissig, H., Shindyalov, I. N., and Bourne, P. E. (2000) The Protein Data Bank. *Nucleic Acids Res. 28*, 235–242.
2. Krentz, A. J., and Bailey, C. J. (2005) Oral antidiabetic agents—Current role in type 2 diabetes mellitus. *Drugs 65*, 385–411.
3. Mooradian, A. D., and Thurman, J. E. (1999) Drug therapy of postprandial hyperglycaemia. *Drugs 57*, 19–29.
4. Scott, L. J., and Spencer, C. M. (2000) Miglitol—A review of its therapeutic potential in type 2 diabetes mellitus. *Drugs 59*, 521–549.
5. Chiasson, J. L., Josse, R. G., Hunt, J. A., Palmason, C., Rodger, N. W., Ross, S. A., Ryan, E. A., Tan, M. H., and Wolever, T. M. S. (1994) The efficacy of acarbose in the treatment of patients with non-insulin-dependent diabetes-mellitus—A multicenter controlled clinical-trial. *Ann. Intern. Med. 121*, 928–935.
6. Cantarel, B. L., Coutinho, P. M., Rancurel, C., Bernard, T., Lombard, V., and Henrissat, B. (2009) The Carbohydrate-Active EnZymes database (CAZy): An expert resource for glycogenomics. *Nucleic Acids Res. 37*, D233–D238.
7. Stam, M. R., Danchin, E. G. J., Rancurel, C., Coutinho, P. M., and Henrissat, B. (2006) Dividing the large glycoside hydrolase family 13 into subfamilies: towards improved functional annotations of alpha-amylase-related proteins. *Protein Eng., Des. Sel. 19*, 555–562.
8. Brayer, G. D., Luo, Y. G., and Withers, S. G. (1995) The structure of human pancreatic alpha-amylase at 1.8 angstrom resolution and comparisons with related enzymes. *Protein Sci. 4*, 1730–1742.

9. Numao, S., Maurus, R., Sidhu, G., Wang, Y., Overall, C. M., Brayer, G. D., and Withers, S. G. (2002) Probing the role of the chloride ion in the mechanism of human pancreatic alpha-amylase. *Biochemistry 41*, 215–225.
10. Maurus, R., Begum, A., Kuo, H. H., Racaza, A., Numao, S., Andersen, C., Tams, J. P., Vind, J., Overall, C. M., Withers, S. G., and Brayer, G. D. (2005) Structural and mechanistic studies of chloride induced activation of human pancreatic alpha-amylase. *Protein Sci. 14*, 743–755.
11. Maurus, R., Begum, A., Williams, L. K., Fredriksen, J. R., Zhang, R., Withers, S. G., and Brayer, G. D. (2008) Alternative catalytic anions differentially modulate human alpha-amylase activity and specificity. *Biochemistry 47*, 3332–3344.
12. Brayer, G. D., Sidhu, G., Maurus, R., Rydberg, E. H., Braun, C., Wang, Y. L., Nguyen, N. T., Overall, C. H., and Withers, S. G. (2000) Subsite mapping of the human pancreatic alpha-amylase active site through structural, kinetic, and mutagenesis techniques. *Biochemistry 39*, 4778–4791.
13. Li, C. M., Begum, A., Numao, S., Park, K. H., Withers, S. G., and Brayer, G. D. (2005) Acarbose rearrangement mechanism implied by the kinetic and structural analysis of human pancreatic alpha-amylase in complex with analogues and their elongated counterparts. *Biochemistry 44*, 3347–3357.
14. Svensson, B., and Sogaard, M. (1993) Mutational analysis of glycosylase function. *J. Biotechnol. 29*, 1–37.
15. Rydberg, E. H., Li, C. M., Maurus, R., Overall, C. M., Brayer, G. D., and Withers, S. G. (2002) Mechanistic analyses of catalysis in human pancreatic alpha-amylase: Detailed kinetic and structural studies of mutants of three conserved carboxylic acids. *Biochemistry 41*, 4492–4502.
16. Zechel, D. L., and Withers, S. G. (2000) Glycosidase mechanisms: Anatomy of a finely tuned catalyst. *Acc. Chem. Res. 33*, 11–18.
17. Davies, G. J., Mackenzie, L., Varrot, A., Dauter, M., Brzozowski, A. M., Schulein, M., and Withers, S. G. (1998) Snapshots along an enzymatic reaction coordinate: Analysis of a retaining beta-glycoside hydrolase. *Biochemistry 37*, 11707–11713.
18. Ducros, V. M. A., Zechel, D. L., Murshudov, G. N., Gilbert, H. J., Szabo, L., Stoll, D., Withers, S. G., and Davies, G. J. (2002) Substrate distortion by a beta-mannanase: Snapshots of the Michaelis and covalent-intermediate complexes suggest a B-2,B-5 conformation for the transition state. *Angew. Chem., Int. Ed. 41*, 2824–2827.
19. Vocadlo, D. J., and Davies, G. J. (2008) Mechanistic insights into glycosidase chemistry. *Curr. Opin. Chem. Biol. 12*, 539–555.
20. Vocadlo, D. J., Davies, G. J., Laine, R., and Withers, S. G. (2001) Catalysis by hen egg-white lysozyme proceeds via a covalent intermediate. *Nature 412*, 835–838.
21. Uitdehaag, J. C. M., Mosi, R., Kalk, K. H., van der Veen, B. A., Dijkhuizen, L., Withers, S. G., and Dijkstra, B. W. (1999) X-ray structures along the reaction pathway of cyclodextrin glycosyltransferase elucidate catalysis in the alpha-amylase family. *Nat. Struct. Biol. 6*, 432–436.
22. Jensen, M. H., Mirza, O., Albenne, C., Remaud-Simeon, M., Monsan, P., Gajhede, M., and Skov, L. K. (2004) Crystal structure of the covalent intermediate of amylosucrase from *Neisseria polysaccharea*. *Biochemistry 43*, 3104–3110.
23. Barends, T. R. M., Bultema, J. B., Kaper, T., van der Maarel, M. J. E. C., Dijkhuizen, L., and Dijkstra, B. W. (2007) Three-way stabilization of the covalent intermediate in amylomaltase, an alpha-amylase-like transglycosylase. *J. Biol. Chem. 282*, 17242–17249.
24. Woo, E. J., Lee, S., Cha, H., Park, J. T., Yoon, S. M., Song, H. N., and Park, K. H. (2008) Structural insight into the bifunctional mechanism of the glycogen-debranching enzyme TreX from the archaeon *Sulfolobus solfataricus*. *J. Biol. Chem. 283*, 28641–28648.
25. Rempel, B. P., and Withers, S. G. (2008) Covalent inhibitors of glycosidases and their applications in biochemistry and biology. *Glycobiology 18*, 570–586.
26. Braun, C., Brayer, G. D., and Withers, S. G. (1995) Mechanism-based inhibition of yeast alpha-glucosidase and human pancreatic alpha-amylase by a new class of inhibitors—2-Deoxy-2,2-difluoro-alpha-glycosides. *J. Biol. Chem. 270*, 26778–26781.
27. Hart, D. O., He, S. M., Chany, C. J., Withers, S. G., Sims, P. F. G., Sinnott, M. L., and Brumer, H. (2000) Identification of Asp-130 as the catalytic nucleophile in the main alpha-galactosidase from *Phanerochaete chrysosporium*, a family 27 glycosyl hydrolase. *Biochemistry 39*, 9826–9836.
28. Zhang, R., McCarter, J. D., Braun, C., Yeung, W., Brayer, G. D., and Withers, S. G. (2008) Synthesis and testing of 2-deoxy-2,2-dihaloglycosides as mechanism-based inhibitors of alpha-glycosidases. *J. Org. Chem. 73*, 3070–3077.
29. McCarter, J. D., and Withers, S. G. (1996) 5-fluoro glycosides: A new class of mechanism-based inhibitors of both alpha- and beta-glucosidases. *J. Am. Chem. Soc. 118*, 241–242.
30. McCarter, J. D., and Withers, S. G. (1996) Unequivocal identification of Asp-214 as the catalytic nucleophile of *Saccharomyces cerevisiae* alpha-glucosidase using 5-fluoro glycosyl fluorides. *J. Biol. Chem. 271*, 6889–6894.
31. Hagena, T. L., and Coward, J. K. (2009) Fluoridolysis of 5,6-epoxy carbohydrates: Application to the synthesis of 5-fluoro lactosamine and isolactosamine glycosides. *Tetrahedron: Asymmetry 20*, 781–794.
32. Rydberg, E. H., Sidhu, G., Vo, H. C., Hewitt, J., Cote, H. C. F., Wang, Y. L., Numao, S., MacGillivray, R. T. A., Overall, C. M., Brayer, G. D., and Withers, S. G. (1999) Cloning, mutagenesis, and structural analysis of human pancreatic alpha-amylase expressed in *Pichia pastoris*. *Protein Sci. 8*, 635–643.
33. Damager, I., Numao, S., Chen, H. M., Brayer, G. D., and Withers, S. G. (2004) Synthesis and characterisation of novel chromogenic substrates for human pancreatic alpha-amylase. *Carbohydr. Res. 339*, 1727–1737.
34. Otwinowski, Z., and Minor, W. (1997) Processing of X-ray diffraction data collected in oscillation mode. *Methods Enzymol. 276*, 307–326.
35. Burk, D., Wang, Y. L., Dombroski, D., Berghuis, A. M., Evans, S. V., Luo, Y. G., Withers, S. G., and Brayer, G. D. (1993) Isolation, crystallization and preliminary diffraction analyses of human pancreatic alpha-amylase. *J. Mol. Biol. 230*, 1084–1085.
36. Brunger, A. T., Adams, P. D., Clore, G. M., DeLano, W. L., Gros, P., Grosse-Kunstleve, R. W., Jiang, J. S., Kuszewski, J., Nilges, M., Pannu, N. S., Read, R. J., Rice, L. M., Simonson, T., and Warren, G. L. (1998) Crystallography & NMR system: A new software suite for macromolecular structure determination. *Acta Crystallogr. 54*, 905–921.
37. Jones, T. A., Zou, J. Y., Cowan, S. W., and Kjeldgaard, M. (1991) Improved methods for building protein models in electron density maps and the location of errors in these models. *Acta Crystallogr. A 47* (Part 2), 110–119.
38. Numao, S., Damager, I., Li, C. M., Wrodnigg, T. M., Begum, A., Overall, C. M., Brayer, G. D., and Withers, S. G. (2004) In situ extension as an approach for identifying novel alpha-amylase inhibitors. *J. Biol. Chem. 279*, 48282–48291.
39. Numao, S., Kuntz, D. A., Withers, S. G., and Rose, D. R. (2003) Insights into the mechanism of *Drosophila melanogaster* Golgi alpha-mannosidase II through the structural analysis of covalent reaction intermediates. *J. Biol. Chem. 278*, 48074–48083.
40. Blanchard, J. E., and Withers, S. G. (2001) Rapid screening of the aglycone specificity of glycosidases: Applications to enzymatic synthesis of oligosaccharides. *Chem. Biol. 8*, 627–633.
41. Qian, M. X., Haser, R., Buisson, G., Duee, E., and Payan, F. (1994) The active-center of a mammalian alpha-amylase—Structure of the complex of a pancreatic alpha-amylase with a carbohydrate inhibitor refined to 2.2-angstrom resolution. *Biochemistry 33*, 6284–6294.
42. Qian, M. X., Spinelli, S., Driguez, H., and Payan, F. (1997) Structure of a pancreatic alpha-amylase bound to a substrate analogue at 2.03 angstrom resolution. *Protein Sci. 6*, 2285–2296.
43. Biarnes, X., Ardevol, A., Planas, A., Rovira, C., Laio, A., and Parrinello, M. (2007) The conformational free energy landscape of beta-D-glucopyranose. Implications for substrate preactivation in beta-glucoside hydrolases. *J. Am. Chem. Soc. 129*, 10686–10693.
44. DeLano, W. L. (2002) The PyMOL Molecular Graphics System, Delano Scientific, San Carlos, CA (http://www.pymol.org).